Nonequilibrium molecular dynamics simulations of heat flow in one-dimensional lattices

Fei Zhang,[1] Dennis J. Isbister,[1] and Denis J. Evans[2]
[1]*School of Physics, University of New South Wales, University College, ADFA, Canberra, ACT 2612, Australia*
[2]*Research School of Chemistry, Australian National University, Canberra, ACT 0200, Australia*
(Received 18 October 1999)

We study the use of the Evans nonequilibrium molecular dynamics (NEMD) heat flow algorithm for the computation of the heat conductivity in one-dimensional lattices. For the well-known Fermi-Pasta-Ulam model, it is shown that when the heat field strength is greater than a certain critical value (which depends on the system size) solitons can be generated in molecular dynamics simulations starting from random initial conditions. Such solitons are stable and travel with supersonic speeds. For smaller heat fields, no solitons are generated in the molecular dynamics simulations; the heat conductivity obtained via the NEMD algorithm increases monotonically with the size of the system.

PACS number(s): 05.70.Ln, 05.45.Yv, 44.10.+i, 05.60.−k

I. INTRODUCTION

Heat conduction in one-dimensional (1D) lattices has attracted much research interest. Surprisingly, it has been found that many 1D lattices do not obey the Fourier's law [1–17]: the thermal conductivity is divergent in the thermodynamic limit. For harmonically coupled oscillators, it was rigorously shown that the thermal conductivity λ is proportional to the number of oscillators N [1]. Such a divergence is founded in the existence of extended waves (phonons) freely traveling (and carrying thermal energy) along the lattice without attenuation. In later studies [2,3], impurities or defects in the chain were taken into account, since it was anticipated that phonon waves could be damped by the scattering processes due to such defects, thus possibly removing the N divergence of λ. However, it was demonstrated for isotopically disordered harmonic chains that the heat conductivity still diverged at a somewhat slower rate ($\lambda \approx N^{1/2}$) [2,3]. Another way of trying to achieve normal heat conduction in one-dimensional lattices is by invoking anharmonicity [4]: here nonlinearity makes it possible for phonons to interact among themselves thus impeding their free propagation. However, Lepri *et al.* [12] have found that even strong nonlinearity and chaotic behavior is insufficient to ensure the existence of normal heat conduction. In the well-known Fermi-Pasta-Ulam (FPU) β model they found a power-law divergence of the thermal conductivity $\lambda \propto N^{\gamma}$ for $\gamma \approx 0.4$. This power-law divergence was qualitatively attributed to the long-time tail of the heat flux autocorrelation function, whose time integral gives the thermal conductivity of the system [13].

Previous studies of heat conductivity have used a straightforward simulation method [6–17]. In molecular dynamics (MD) simulations two heat reservoirs with high and low temperatures T_H and T_L, respectively, are located on each side of the lattice. The average heat flux and the internal temperature gradient are measured, with the thermal conductivity being the ratio of these two quantities. However, there are a number of disadvantages with this approach. In particular, the system is spatially inhomogeneous and one cannot define an intrinsic temperature T for the system due to the large temperature gradient. Consequently it is impossible to obtain the T dependence of the heat conductivity. In addition, problems associated with the use of the Nosé-Hoover thermostat for boundary particles have been discussed in Ref. [15].

Recently Maeda and Munakata [10] proposed a homogeneous nonequilibrium molecular-dynamics (NEMD) method based on the Evans heat flow algorithm [18–20]. However, the system size used in Ref. [10] was too small (32 particles) to allow one to study the behavior of the NEMD algorithm in the thermodynamic limit.

In this paper we present a detailed study of the Evans NEMD heat flow algorithm for one-dimensional lattices. We demonstrate that when the heat field is sufficiently large, well-defined solitary waves (solitons) can be generated in simulations with random initial conditions. These soliton objects travel at a supersonic speeds, and they also appear in the corresponding Hamiltonian systems. When a soliton is generated, the normal process of homogeneous heat conduction is destroyed, as heat is transferred through the chain via the highly localized solitary wave. This results in a sharp increase in the effective thermal conductivity of the system. Due to this instability, progressively smaller fields are required, as the system size increases, to observe the linear regime of the thermal conductivity and thereby carry out the extrapolation of the thermal conductivity to zero field strength.

The paper is organized as follows. In Sec. II we describe the NEMD equations of motion for one-dimensional lattices with nearest-neighbor interactions, and we point out the possibility of solitary wave solutions in the system. In Sec. III we carry out the nonequilibrium heat flow simulations on the well-known Fermi-Pasta-Ulam model. We show that for the heat field strengths greater than a certain critical value, which depends on the system size and temperature, solitons can be generated from random initial conditions. For smaller heat fields, no solitons can be generated in molecular dynamics simulations with random initial conditions; in this case, the heat conductivity can be obtained via the NEMD algorithm. Some concluding remarks are presented in Sec. IV.

II. NEMD EQUATIONS AND SOLITARY WAVE SOLUTIONS

We consider a 1D system of N particles located along the x axis with lattice constant $a=1$. Each particle is allowed to

move in the y direction, perpendicular to the x axis, and we denote by q_i the displacement of the ith particle and by p_i the corresponding momentum. The Hamiltonian of the system is expressed as

$$\mathcal{H}=\sum_{i=1}^{N}\left[\frac{1}{2m_i}p_i^2+U(q_{i+1}-q_i)\right], \tag{1}$$

where m_i is the mass of the ith particle, and U represents the interparticle interaction potential. For example, the FPU β model is exemplified by $U(r)=\frac{1}{2}r^2+\beta/4r^4$, $r\equiv q_{i+1}-q_i$.

The Evans thermal conductivity algorithm for general N-particle systems of fluid has been described in detail [18,19]. The basis of this algorithm is the Green-Kubo relation for the thermal conductivity. For a 1D system defined by the Hamiltonian model (1), the thermal conductivity coefficient is given by [19]

$$\lambda=\lim_{\tau\to\infty}\frac{L}{k_BT^2}\int_0^\tau dt\langle J_x(t)J_x(0)\rangle_{\rm eq}, \tag{2}$$

where k_B is the Boltzmann's constant, T is the absolute temperature of the system, and $L=Na$ is the system size. (The lattice spatial constant a is taken to be 1 in this paper.) The notation $\langle\cdots\rangle_{\rm eq}$ denotes an equilibrium ensemble average. The heat flux vector J_x is given by

$$J_x(t)=-\frac{1}{2N}\sum_i\frac{p_i}{m_i}[U'(q_{i+1}-q_i)+U'(q_i-q_{i-1})]. \tag{3}$$

In the Evans NEMD algorithm the N particle system is coupled to a ''heat field'' F_e. The coupling is defined in such a way that the energy dissipation is proportional to J_xF_e, i.e., $d\mathcal{H}/dt=LJ_xF_e$, and that the adiabatic incompressibility of phase space ($AI\Gamma$) condition is satisfied [19]. The thermal conductivity coefficient can then be found from the ratio of the heat flux to the applied heat field

$$\lambda=\lim_{F_e\to0}\lim_{t\to\infty}\frac{\langle J_x(t)\rangle}{TF_e}. \tag{4}$$

Here $\langle J_x(t)\rangle$ is, in principle, a nonequilibrium ensemble average; but in practice, it can be replaced by a time average of $J_x(t)$ if the nonequilibrium steady state is unique. As pointed out in the literature (e.g., Ref. [19]), this heat flow algorithm is only valid in the linear regime, i.e., $|F_e|\to0$. In the nonlinear regime when F_e is not so small (problem dependent), there is no known physical meaning or interpretation for the quantity, $\lim_{t\to\infty}\langle J_x(t)\rangle/TF_e$.

The equations of motion which satisfy the above conditions are

$$\dot{q}_i=p_i/m_i, \tag{5}$$

$$\dot{p}_i=F_i+F_eD_i-\alpha p_i, \tag{6}$$

where $F_i=U'(q_{i+1}-q_i)-U'(q_i-q_{i-1})$ is the total force on particle i due to the nearest-neighbor interaction

$$D_i=-\frac{1}{2}[U'(q_{i+1}-q_i)+U'(q_i-q_{i-1})]+\frac{1}{N}\sum_{j=1}^{N}U'(q_{j+1}-q_j), \tag{7}$$

and α is the thermostat multiplier. For a Gaussian thermostat, α is

$$\alpha=\frac{1}{2K_0}\sum_{j=1}^{N}\frac{p_j}{m_j}(F_j+F_eD_j),\quad K_0=\frac{1}{2}\sum_{j=1}^{N}p_j^2/m_j. \tag{8}$$

This Gaussian thermostat ensures that the system's kinetic energy is fixed at the constant value K_0. We note that the total force exerted on the system is exactly zero, i.e., $\Sigma_i(F_i+F_eD_i)=0$. Thus the total momentum, $\Sigma p_i(t)$, will remain zero for $t>0$ provided that its initial value vanishes.

We have simulated the above described NEMD equations (5)–(8) for a variety of interparticle interaction potentials, and we observe well-defined solitary wave excitations. Before describing our numerical results we first analyze why such solitary waves can occur.

For simplicity, we set $m_i=1$ for all i. From Eqs. (5) and (6) we obtain

$$\ddot{q}_i=F_i+F_eD_i-\alpha\dot{q}_i. \tag{9}$$

Introducing a new variable $Q_i=q_i-q_{i-1}$, leads to

$$\begin{aligned}\ddot{Q}_i&=F_i-F_{i-1}+F_e(D_i-D_{i-1})-\alpha\dot{Q}_i\\&\equiv U'(Q_{i+1})-2U'(Q_i)+U'(Q_{i-1})\\&\quad-\frac{1}{2}F_e[U'(Q_{i+1})-U'(Q_{i-1})]-\alpha\dot{Q}_i.\end{aligned} \tag{10}$$

This equation, together with Eq. (8) for the definition of α, forms a set of lattice equations for the variable Q_i. Note that if F_e and α are set equal to zero, then Eq. (10) becomes a lattice system which can support stable supersonic solitary waves for many types of nearest-neighbor interaction potentials U (see, e.g., Refs. [21–26]). But exact analytical solutions for the solitary waves are not available except for some rather special potential functions U. For example, in the Toda lattice, $U(r)=(b/a)[\exp(-ar)+ar-1]$, the system is integrable and exact analytical soliton solutions are known [21].

To analyze Eq.(10) we can use the so-called quasicontinuum approximation techniques of Refs. [21–26] to reduce Eq. (10) to a partial differential equation

$$\left[\frac{\partial^2}{\partial t^2}+\alpha\frac{\partial}{\partial t}\right]Q=\left[\frac{\partial^2}{\partial x^2}+\frac{1}{12}\frac{\partial^4}{\partial x^4}-F_e\left(\frac{\partial}{\partial x}+\frac{1}{6}\frac{\partial^3}{\partial x^3}\right)\right]U'(Q),\quad x\in[0,L] \tag{11}$$

which can be considered as a generalized Boussinesq equation [24]. Here due to the periodic boundary conditions used for the system (5),(6), i.e., $q_{N+1}=q_1$, The solution of Eq. (11) must satisfy

$$\int_0^L Q(x)dx\equiv0. \tag{12}$$

We assume that $Q(x,t)=Q_s(x-Vt)+Q_0$, where Q_0 is a constant background and Q_s is a localized soliton profile which vanishes as $z=x-Vt\to\pm\infty$. Then from Eq. (12) we have

$$Q_0=-\frac{1}{L}\int_0^L Q_s(x-Vt)dx. \tag{13}$$

Substituting $Q(x,t)=Q_s(x-Vt)+Q_0$ into Eq. (11) we find that the solitary wave profile $Q_s(z)=Q_s(x-Vt)$ should satisfy

$$\left[V^2\frac{\partial^2}{\partial z^2}-\alpha V\frac{\partial}{\partial z}\right]Q_s=\left[\frac{\partial^2}{\partial z^2}+\frac{1}{12}\frac{\partial^4}{\partial z^4}-F_e\left(\frac{\partial}{\partial z}+\frac{1}{6}\frac{\partial^3}{\partial z^3}\right)\right]U'(Q_s+Q_0). \tag{14}$$

It does not seem possible to find an analytical solution for this differential equation for the general case of $Q_0\neq 0$, $F_e\neq 0$, and $\alpha\neq 0$.

However, we note that if the system is large ($N\gg 1$) then Q_0 must be very small according to Eq. (13). Moreover, assuming that F_e and α are small parameters, we can set $Q_0=0$, $F_e=0$, and $\alpha=0$ in Eq. (14). After such a drastic simplification, it is possible to find approximate solitary wave solutions analytically for various types of interparticle potentials $U(Q)$ [21–26]. Here we consider a particular example, the FPU potential $U(Q)=\frac{1}{2}Q^2+\frac{1}{4}\beta Q^4$. According to Refs. [26], the solitary wave profile $Q(z)$ can be approximated by

$$Q_s(z)=\pm\sqrt{\frac{2(V^2-1)}{\beta}}\,\mathrm{sech}[2z\sqrt{(V^2-1)/V^2}]. \tag{15}$$

Once such an approximate soliton solution is obtained then we can transform to the original lattice variables (q_i,p_i). Notice that $Q_i=q_i-q_{i-1}$, thus

$$q_i=q_0+\sum_{j=1}^{i}Q_j\approx q_0+\int_0^z[Q_0+Q_s(x-Vt)]dx. \tag{16}$$

Consequently, the contribution to the kinetic energy from the soliton is

$$\begin{aligned}K_{\mathrm{sol}}&=\frac{1}{2}\sum p_i^2=\frac{1}{2}\sum \dot{q}_i^2\\&\approx\frac{1}{2}\int_{-\infty}^{\infty}dz\left[\int_0^z VQ_s'(x-Vt)dx\right]^2\\&=\frac{1}{2}V^2\int_{-\infty}^{\infty}Q_s^2(z)dz\\&=V^3\sqrt{\frac{V^2-1}{\beta}}.\end{aligned} \tag{17}$$

In numerical simulation we observe that when a soliton is generated, small amplitude phonon waves give a negligible contribution to the system's kinetic energy. In such a case, we have

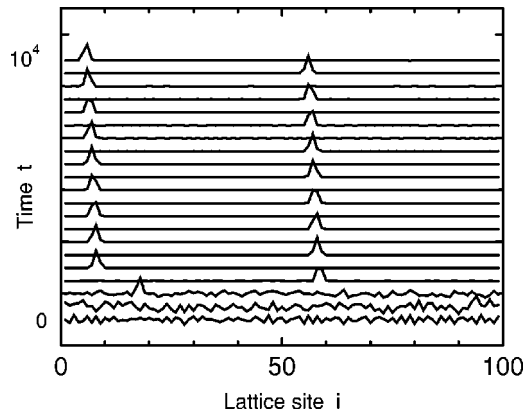

FIG. 1. The evolution of $Q_i(t)=q_{i+1}(t)-q_i(t)$, showing the generation of a solitary wave in a NEMD simulation of heat flow in the FPU β model. The heat field strength is $F_e=0.006$, the system size is $N=100$ particles, and the simulation temperature is $T=1$. Note that due to the periodic boundary conditions the soliton enters into the left end of the lattice whenever it leaves the right end; units are dimensionless for the quantities plotted in this and all other figures.

$$V^3\sqrt{\frac{V^2-1}{\beta}}=K_0\equiv\frac{(N-2)T}{2}, \tag{18}$$

where T is the absolute temperature of the system which is fixed by the Gaussian thermostat. (Here the Boltzmann constant k_B is set to be 1.) For any values of N and T, Eq. (18) has a unique solution $V>1$, which is the (supersonic) speed of the solitary wave. Moreover, according to Eq. (18), the soliton speed increases with the system's total kinetic energy. In the next section, we present numerical simulation results to confirm these analytical predictions.

III. SIMULATION RESULTS

Following Ref. [10] we apply the NEMD heat flow algorithm [Eqs. (5),(6)] to the FPU β-model for which $U_{\mathrm{FPU}}(r)=r^2/2+\beta r^4/4$, and the parameter β is taken to be 1 without

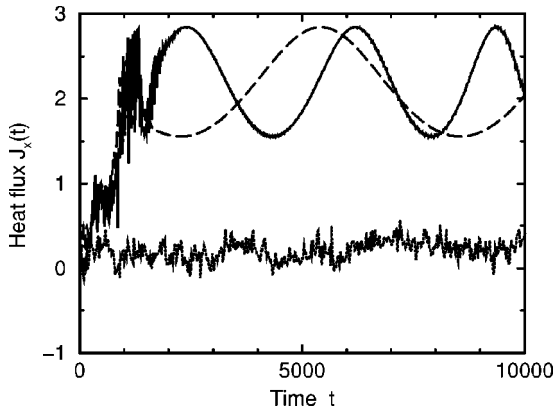

FIG. 2. The instantaneous heat flux in NEMD simulations of heat flow in the FPU model, with $F_e=0.006$ (solid line) and $F_e=0.01$ (long dashed), showing a drastic increase of heat flux when a soliton is generated about time $t=1000$ in both cases. This is in contrast to the situation when no soliton is generated for $F_e=0.002$ (dotted line). The system size is $N=100$ particles and the simulation temperature is T=1.

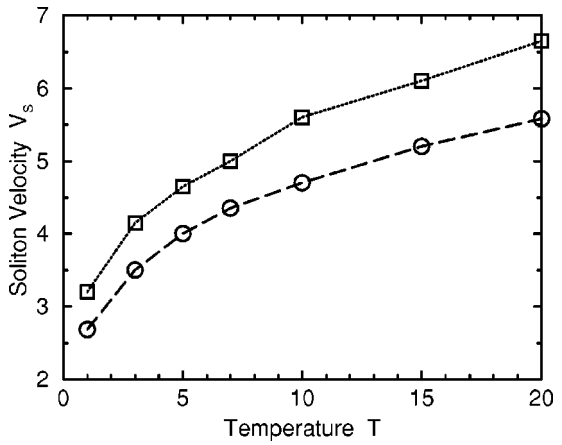

FIG. 3. The velocity of the solitons generated in the FPU lattice with N=100 particles (circles) and $N=200$ particles (squares), respectively. The heat field strength is $F_e=0.01$. Lines are for guidance only.

loss of generality. Periodic boundary conditions are always used. Unless indicated otherwise, the initial conditions for q_i and p_i are obtained by a random number generator. The equations of motion are integrated using a fourth-order operator-splitting integrator which conserves the system's kinetic energy [27]. The time step size is $\delta t=0.005$ and the total simulation time is between 10^4-10^6 units for each trajectory.

The first feature of note is that for a given temperature T and particle number N, stable solitary waves can be generated during simulations (which start from random initial conditions) *if* the heat field strength F_e is greater than a certain critical value F_{cr}. The solitary wave travels in the direction of heat flow (to the right in Fig. 1) with a supersonic speed ($V_s>1$). When the soliton is generated the normal process of homogeneous heat conduction is destroyed and the heat flux increases drastically (Fig. 2). In such a case, heat is transported in the form of a highly localized energy pulse carried by the soliton, and the average value of heat flux is nearly independent of F_e. (Note that all units are dimensionless for quantities plotted in Figs. 1–9 in this paper.)

We find that the soliton's velocity increases with temperature and system size (Fig. 3), but it is nearly independent of the heat field strength $F_e(\leqslant 1.0)$. For example, for $N=100,T=10$, the soliton's velocity is found to be, 4.7, 4.7, and 4.8 for $F_e=0.01,0.1$, and 1.0, respectively. This is in good *qualitative* agreement with that predicted by Eq. (18). In addition, it is found that the analytical result (18) gives very good estimates for the soliton's velocity. For instance, for $N=200,T=1$, Eq. (18) gives $V=3.195$; in the numerical simulation we found that the soliton's velocity is about 3.2. Similar as the case for Hamiltonian lattices [21–26], we find that the soliton's amplitude increases with its velocity.

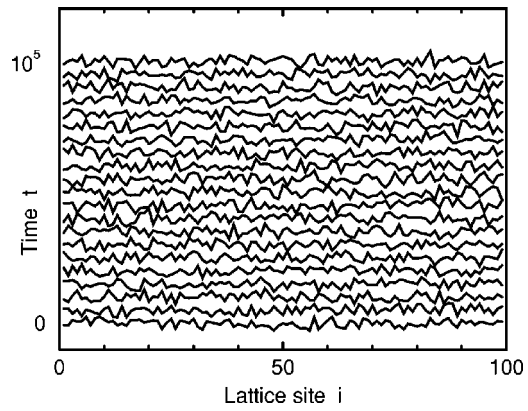

FIG. 5. The evolution of $Q_i(t)=q_{i+1}(t)-q_i(t)$, showing that no soliton is generated for a small heat field strength $F_e=0.002$, which is below the critical value.

Although the spontaneous generation of solitary waves (from random initial conditions) is observed in the NEMD simulations *only when* the heat field is strong enough, such waves, once generated, continue to exist in the system after the heat field and thermostat are *switched off* (Fig. 4). The reason for such a behavior is that the soliton is an inherent excitation in the FPU β model, as explained in the previous section.

When the heat field strength F_e is smaller than the critical value no soliton can be generated from random initial conditions (see Fig. 5). In this case, the time-averaged heat flux $\langle J_x(t)\rangle$ can be measured (see Fig. 6), and the conductivity, $\lim_{t\to\infty}\langle J_x(t)\rangle/(TF_e)$, can be calculated. In Fig. 7 the heat conductivity obtained through the NEMD simulations is plotted (error bars are estimated to be within 10% at most). The NEMD heat conductivity increases with the system size.

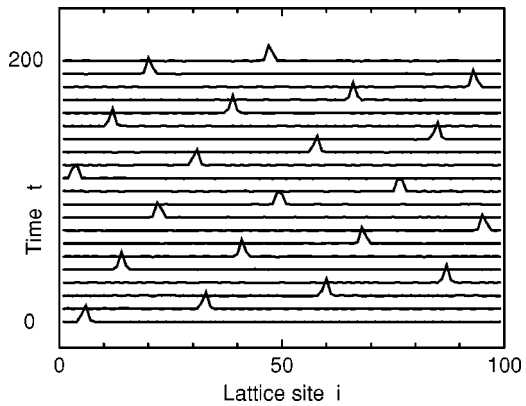

FIG. 4. Propagation of a soliton in the Hamiltonian FPU lattice, which has no applied heat field ($F_e=0.0$) and thermostat ($\alpha=0$). The initial conditions are taken from the last output of Fig. 1.

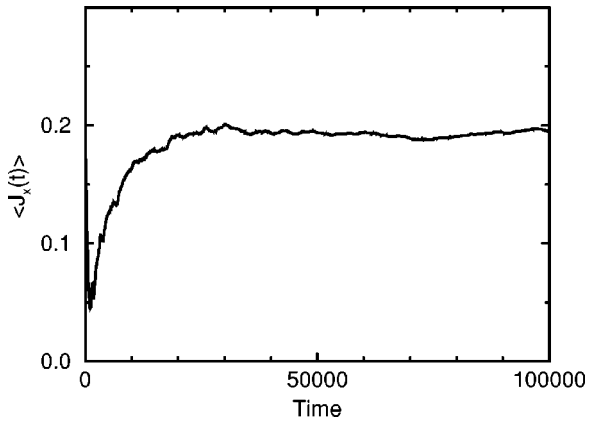

FIG. 6. Time-averaged heat flux in a NEMD simulation of heat flow in the FPU model. $F_e=0.002$, $N=100,T=1$.

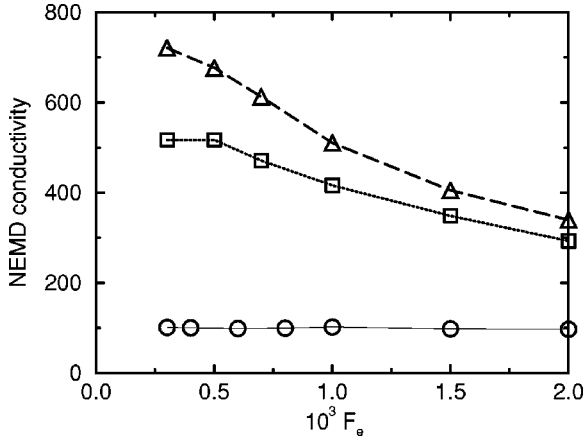

FIG. 7. The heat conductivity obtained from the NEMD simulation of the FPU lattice with $N=100$ (circles), 300 (squares), and 400 (triangles) particles, respectively. The simulation temperature is $T=1$. Lines are for guidance only.

When $F_e \to 0$ the conductivity converges to a finite value, which, according to the generalized Green-Kubo relation [19,28], should equal the conductivity obtained through Eq. (2). We have tested this convergence for the FPU system of $N=100$ particles. In Fig. 8 we plot the function

$$\lambda(t)=\frac{N}{k_B T^2}\int_0^t d\tau \langle J_x(\tau)J_x(0)\rangle_{\rm eq}, \tag{19}$$

where the ensemble average is obtained by using ten independent trajectories of the length 10^6 units in time. It is clear that when $t\to\infty$, λ approaches to a value around 93, which is in good agreement with the heat conductivity obtained through NEMD algorithm (see Fig. 7).

Finally, we investigate how the critical field strength $F_{\rm cr}$ for generating solitons depends on the particle number N and the system temperature T. We found that $F_{\rm cr}$ increases with T. For example, at $N=100$ the critical value $F_{\rm cr}$ is around 0.0054 and 0.0085 for $T=1$ and $T=10$, respectively. On the other hand, we found that $F_{\rm cr}$ decreases monotonically with N as shown in Fig. 9. For a system of 10 000 particles, the critical field is as small as 0.0005 (accuracy is within $\pm 10^{-4}$). This means that an extremely small field has to be used in order to observe the linear regime (with no solitons) of heat conduction. However, when the heat field is too small

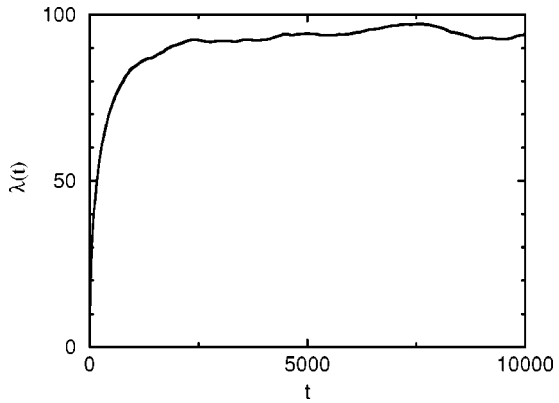

FIG. 8. The time-dependent heat conductivity $\lambda(t)$ calculated from the Green-Kubo formula (19), for the FPU lattice with $N=100$ particles, and temperature $T=1$.

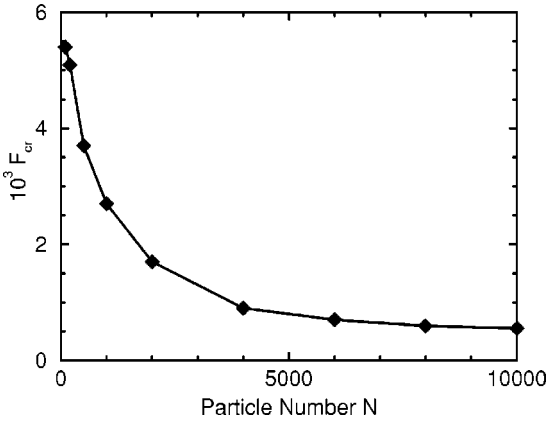

FIG. 9. The critical field strength for generating solitons, as a function of the particle number. The simulation temperature is $T=1$. The line is for guidance only.

the noise-signal ratio [when using Eq. (4)] would become too large and thus the efficiency of the NEMD algorithm will be drastically reduced.

IV. CONCLUDING REMARKS

In conclusion, we have shown that the Evans NEMD heat flow algorithm, which was designed originally for computing thermal conductivity in liquids, can generate solitons when it is applied to 1D lattices. In the well-known FPU model, we have shown that when the heat field strength is greater than a certain critical value a soliton can be generated from random initial conditions. Such a soliton is stable and it travels with a supersonic speed which is determined by the system size and temperature. Because of this instability, progressively smaller fields have to be used (as the system size increases) to observe the linear regime of the thermal conductivity and thereby carry out the extrapolation to zero field. This greatly reduces the efficiency with which the algorithm can be used to compute the thermal conductivity of large 1D lattices. Nevertheless, for small systems, we have found that the heat conductivity increases with the size of the system, which is in qualitative agreement with previous findings [12–14].

The present study has been primarily focused on FPU β model, but we have checked numerically that similar phenomena also exist for other types of 1D lattices with distinct interparticle interaction potentials (e.g., the Toda potential and Morse potential) and even for diatomic lattices. In particular, the spontaneous generation of solitons can be observed not only for the nonequilibrium heat flow systems with Gaussian thermostat but also with the Nosé-Hoover thermostat and an isoenergetic thermostat. The mechanism underlying the observed chaos-soliton transition above the critical field strength still remains to be identified, particularly in terms of Lyapunov spectra-shift and phase space contraction [19] induced by the nonequilibrium heat flow algorithms. This and other related issues will be addressed in our future work [29].

ACKNOWLEDGMENT

We thank Debra J. Searles and Professor E. G. D. Cohen for useful discussions and comments about this work. This work was supported by ARC Large Grant No. A69800064.

[1] Z. Rieder and J. L. Lebowitz, J. Math. Phys. **8**, 1073 (1967).
[2] H. Matsuda and K. Ishii, Suppl. Prog. Theor. Phys. **45**, 56 (1970).
[3] J.B. Keller, G.C. Papanicolaou, and J. Weilenmann, Commun. Pure Appl. Math. **32**, 583 (1978).
[4] R.E. Peierls, *Quantum Theory of Solids* (Oxford University Press, London, 1955).
[5] F. Mokross and H. Buttner, J. Phys. C **16**, 4539 (1983).
[6] G. Casati, J. Ford, F. Vivaldi, and W. M. Visscher, Phys. Rev. Lett. **52**, 1861 (1984).
[7] M. Mareschal and A. Amellal, Phys. Rev. A **37**, 2189 (1988).
[8] E.A. Jackson and A. D. Mistriotis, J. Phys.: Condens. Matter **1**, 1223 (1989).
[9] H. Kaburaki and M. Machida, Phys. Lett. A **181**, 85 (1993).
[10] A. Maeda and T. Munakata, Phys. Rev. E **52**, 234 (1995).
[11] D. J. Mimnagh and L. E. Ballentine, Phys. Rev. E **56**, 5332 (1997).
[12] S. Lepri, R. Livi, and A. Politi, Phys. Rev. Lett. **78**, 1896 (1997); Physica D **119**, 140 (1998).
[13] S. Lepri, R. Livi, and A. Politi, Europhys. Lett. **43**, 271 (1998).
[14] B. Hu, B. Li, and H. Zhao, Phys. Rev. E **57**, 2992 (1998).
[15] A. Fillipov, B. Hu, B. W. Li, and A. Zeltser, J. Phys. A **31**, 7719 (1998).
[16] H. A. Posch and Wm. G. Hoover, Phys. Rev. E **58**, 4344 (1998).
[17] T. Hatano, Phys. Rev. E **59**, R1 (1999).
[18] D. J. Evans, Phys. Lett. **91A**, 457 (1982).
[19] D. J. Evans and G. P. Morriss, *Statistical Mechanics of Nonequilibrium Liquids* (Academic, New York, 1990); see web page at http://www.rsc.anu.edu.au/~evans/evansmorrissbook.htm for an updated version of the book.
[20] D. J. Evans and H. J. M. Hanley, Mol. Phys. **68**, 97 (1989); D. P. Hansen and D. J. Evans, *ibid.* **81**, 767 (1994); D. P. Hansen and D. J. Evans, Mol. Simul. **14**, 409 (1995).
[21] M. Toda, *Theory of Nonlinear Lattices* (Springer-Verlag, Berlin, 1981).
[22] M. A. Collins, Chem. Phys. Lett. **77**, 342 (1981); J. Chem. Phys. **77**, 2607 (1982); Adv. Chem. Phys. **53**, 225 (1983); Phys. Rev. A **31**, 1754 (1985).
[23] P. Rosenau, Phys. Lett. A **118**, 222 (1986).
[24] M. Peyrard, S. Pnevmatikos, and N. Flytzanis, Physica D **19**, 268 (1986); J. Phys. A **22**, 783 (1989).
[25] D. Hochstrasser, F. G. Mertens, and H. Buttner, Physica D **35**, 259 (1989).
[26] J. A. D. Wattis, J. Phys. A **26**, 1193 (1993).
[27] F. Zhang, J. Chem. Phys. **106**, 6102 (1997).
[28] S. Sarman, D. J. Evans, and P. T. Cummings, Phys. Rep. **305**, 1 (1998).
[29] F. Zhang, D.J. Isbister, and D. J. Evans (unpublished).